Experimental Study of Distance Dependence Interference Robustness and Turning Sensitivity in IR Line-Sensor-Based Leader–Follower Control on the 3Pi+ 32U4

2677318 2832689 2707066 2740187

***Abstract*—This report is based on the Pololu 3pi+ 32U4 teaching mobile robot platform and focuses on constructing a Leader-Follower system. The system studied key performance indicators such as distance observability, anti-interference capability, and turning stability. The "modulation + calibration" strategy has been verified to have an anti-interference effect in infrared positioning scenarios. In terms of turning control, the turning perception structure based on the line sensor was replaced with a "bump sensor + dual PID" architecture. The introduction of feedforward speed, first-order low-pass filtering, direction deadband, and increasing the proportional coefficient of the steering PID significantly reduced the distance fluctuations and speed "snake-like" phenomena. It was found that there was significant mutual interference between ADC readings and bump sensor RC Timeout readings on the existing circuit layout. Considering the final system, the RC Timeout of the bump sensor was selected as the distance and direction feedback scheme. To facilitate reproducibility, our source code is publicly available at https://github.com/ChuanXiiiiii/RS-Assessment-2-Leader-Follower.**

I. INTRODUCTION

Most mobile robots are coordinated using leader–follower formation control, where followers maintain a desired distance and bearing from a moving reference [1]. The architecture's local sensing makes it easy and scalable, unlike centralised alternatives. Designing this functionality utilising built-in infrared (IR) sensors instead of LiDAR or cameras for low-cost educational platforms like the Pololu 3Pi+ 32U4 is challenging.

The 3Pi+ 32U4 integrates five downward-facing reflectance line sensors and two forward-facing bump sensors [2]. While the line sensors are typically calibrated for track following and the bump sensors for collision detection, both share similar optoelectronic architectures: they measure the discharge time of a phototransistor–capacitor circuit, which correlates with incident IR intensity [2]. In this project, these sensors are repurposed as short-range photometric detectors. The study explicitly evaluates both the downward-facing line array and the forward-facing bump sensors to determine which configuration offers superior performance for detecting a leader-mounted IR beacon. Sensing relative distance using simple IR intensity is non-trivial compared to Time-of-Flight (ToF) or triangulation systems [3]. The 3Pi+ sensors are not designed for ranging; their response is highly nonlinear and sensitive to geometry. Therefore, before implementing control, it is necessary to characterise how the raw discharge times of both sensor types vary with inter-robot distance. Furthermore, indoor environments introduce interference from broadband IR sources, such as incandescent lights or candle flames, which can saturate sensors [3]. To address this, this project investigates the effect of emitter modulation. The leader robot is programmed with three emission modes—DC (0 Hz), standard PWM (490 Hz), and high-frequency PWM (3.9 kHz)—to evaluate whether higher frequency modulation improves signal-to-noise ratio in the presence of strong interference.

Finally, formation stability during turns depends on the sensor field of view (FOV). The spatial separation between the left and right sensors (both on the line array and the bumper) provides a baseline to estimate heading error [4]. However, this works only within a limited angular range. This research explores whether the differential reading between left and right sensors is sufficient to drive a PID controller for stable following, or if the limited FOV leads to target loss during sharp manoeuvres. Based on the experimental design, this report tests three key hypotheses:

1) **Distance Hypothesis** ($\mathcal{H}_1$): It is hypothesised that for a fixed alignment, the raw discharge times of the follower's IR sensors (both line and bump) will vary monotonically with inter-robot distance over a short operating range. Consequently, a calibration curve can be derived to map these raw readings to distance, enabling a proportional controller to maintain formation.
2) **Anti-Interference Hypothesis** ($\mathcal{H}_2$): Standard DC or low-frequency IR signals are susceptible to environmental noise. It is hypothesised that driving the leader's emitter with high-frequency modulation (3.9 kHz) will yield significantly more stable sensor readings and reduced distance error in the presence of a candle flame compared to DC or standard 490 Hz modulation.
3) **Turning Sensitivity Hypothesis** ($\mathcal{H}_3$): Due to the limited sensor baseline, it is hypothesised that the follower can effectively use the difference between left and right sensor readings to correct heading errors, but only for moderate trajectory curvatures. If the leader's turning rate causes the relative bearing to exceed the effective sensor FOV, the formation is expected to become unstable.

II. IMPLEMENTATION

A. Sensor Configuration and Emission Control

While the hardware layout is standard, the firmware was customised to repurpose the sensors for long-range detection. The Follower was configured to read both the forward-facing Bump Sensors and the downward-facing Line Sensors. To implement the high-frequency emission mode (validating $\mathcal{H}_2$), the Leader's firmware modified the ATmega32U4 `Timer0` prescaler from the default 64 to 8. This adjustment increased the PWM frequency on the emitter pin (Pin 11) from the standard 490 Hz to approximately 3.9 kHz, enabling the evaluation of modulation-based noise rejection without external hardware changes.

B. Signal Measurement Techniques

Two different reading techniques were employed for sensor data acquisition consistent with the timing specification of the sensors [2]:

1) ADC Scaling: The microcontroller's internal ADC within the control loop was used to sample the raw voltage from the phototransistor. The values were all normalized within the range (V_{min}, V_{max}) and scaled to the reference range $S \in [0.0, 1.0]$, ensuring consistent sensitivity regardless of varying lighting conditions [2].

2) Timeout Measurement: To emulate the standard library, firmware measured a small value of time (in μs) when discharging the capacitor. A timeout of 6000μs was used during the measures with no signal present in order to manage the optimization between the loop refresh rate for a real-time control [2].

C. Automated Data Acquisition System

In order to avoid human error for distance hypothesis ($\mathcal{H}_1$) in measurements, an automatic method of logging was established by using the kinematics of the robot. The Follower used its quadrature wheel encoders to measure linear displacement with millimeter resolution, using the manufacturer specified 32mm wheel diameter and gear ratio [1]. A special calibration state ordered the robot to reverse at a constant slow speed and also record odometer readings together with sensor readouts (both ADC and Timeout) to the serial port. This resulted in a dense, continuous dataset for curve fitting.

D. Formation Control

Algorithm A closed-loop formation controller was implemented on the Follower to validate the tracking capability ($\mathcal{H}_3$). The architecture integrates signal pre-processing with a hybrid Feedforward-PID control scheme.

1) Signal Filtering: Raw sensor readings often exhibit high-frequency jitter due to the RC discharge process. A first-order discrete low-pass filter was applied: $S_f(k) = \alpha S_{raw} + (1-\alpha) S_f(k-1)$. The smoothing factor α was empirically tuned to 0.3, balancing noise suppression with response latency.

2) Longitudinal Control (Distance): Linear velocity (v) is regulated by a Distance PID controller acting on the average signal intensity (S_{avg}). To improve responsiveness, a constant feedforward velocity v_{ff} is added to the PID output, a strategy commonly applied to maintain constant spacing in leader-follower platoons [5]:

$$v_{cmd} = v_{ff} + K_p e_d + K_d e_d + Ki \int e_d \tag{1}$$

Where error e_d is the difference between the target intensity and current S_{avg}.

3) Lateral Control (Heading): Angular velocity (ω) is driven by a Heading PID controller based on the differential error between the left and right sensors $e_{\mathrm{h}} = S_{\mathrm{L}} - S_{\mathrm{R}}$. The final motor commands are derived via differential mixing: $v_{\mathrm{L}} = v_{\mathrm{cmd}} - \omega_{\mathrm{turn}}$ and $v_{\mathrm{R}} = v_{\mathrm{cmd}} + \omega_{\mathrm{turn}}$. This mimics the differential steering approach used in line-following AGV formations.

III. EXPERIMENT METHODOLOGY

This section will discuss five experimental methods regarding distance, anti-interference capability and steering sensitivity in this project. Linear sensors and collision sensors are compatible with the Pololu QTR reflective infrared sensor in terms of circuit structure. Two reading methods are supported: RC discharge time and analog voltage (ADC) [1], [6]. These provide the hardware foundation for the length response, modulation frequency anti-interference and steering sensitivity experiments in this project. The leader-follower formation control structure follows the hierarchical control framework of "speed + direction" [1]. The indoor infrared positioning and interference analysis research covers flame detection [3], [7].

A. Overview of Method

Experiment 1 was designed to validate the "distance hypothesis" ($\mathcal{H}_1$). The response curves of the bottom line sensors and front bump sensors were characterized and compared across varying Leader-Follower distances in a static setup.

The Leader robot was fixed at the center of the experimental table and configured to emit infrared signals continuously. The IR emitter (connected to pin `EMIT_PIN`=11) was driven via `analogWrite(128)`, and the prescaler of `Timer0` was set to 8, resulting in a carrier frequency of approximately 3.9 kHz. This high-frequency modulation strategy mitigates interference from ambient DC light and power line flicker.

On the Follower side, all self-emission sources were disabled. Data were sampled from the central bottom line sensor (DN1) and the left and right front bump sensors (phototransistors). Prior to the experiment, the normalization bounds were defined by recording the minimum and maximum RC discharge times under two conditions: "no Leader signal" and "close proximity." Typical raw readings for the line channel ranged from 2452 to 6000 (timeout), while the bump channels exhibited minima of 156–264 and a maximum of 6000.

During measurement, the Leader and Follower were aligned longitudinally. The Follower was manually positioned along a calibrated scale:

- For **line sensor ranging**, measurements were taken from 1 cm to 5 cm at 1 cm intervals.
- For **bump sensor ranging**, measurements spanned 0.5 cm to 12.5 cm, with step sizes varying between 0.5 cm and 1 cm.

Experiment 2 compared the performance of the two infrared receiving structures in the actual ranging-following task based on the results of Experiment 1. This was done to further verify the distance hypothesis and lay the groundwork for the turning sensitivity experiment. The two structures were as follows:

Experiment 2 examined the capabilities of two infrared receiving structures in a ranging-following challenge, based on Experiment 1. It was done to confirm the distance theory and prepare for the turning sensitivity experiment by two structures:

- **B Send B Receive (B→B)**: The Leader uses a forward IR LED to emit, and the Follower uses a forward bump to receive.
- **B Send L Receive (B→L)**: The Leader still uses a forward IR LED, and the Follower switches to using a bottom line sensor to receive.

The Leader continually emits infrared at 3.9 kHz modulation. Both motor speed is 40 PWM. Ensure linear forward movement. The Follower has a twin PID control system, with one PID adjusting linear speed based on distance intensity and the other adjusting differential speed of left and right wheels depending on left and right signal differences [1]. In B→B mode, the Follower disables line sensor output and only detects left and right bumps. In the B→L mode, the bump reading is disabled and only one line sensor is used for reception.

Experiment 3 further designed controller parameter optimization experiments on the B→B structure that performed well, focusing on the distance hypothesis and the turning sensitivity hypothesis. The Follower used the RC discharge times of the left and right bump sensors, normalized them to obtain the left and right intensities S_{L} and S_{R}, and then calculated the average distance intensity $S_{\mathrm{avg}} = (S_{\mathrm{L}} + S_{\mathrm{R}})/2$ and the direction deviation $D = S_{\mathrm{L}} - S_{\mathrm{R}}$. To suppress short-term fluctuations in the RC readings, a first-order discrete low-pass filter was applied to S_{avg}:

$$S_{\mathrm{f}}(k) = \alpha S_{\mathrm{avg}}(k) + (1-\alpha) S_{\mathrm{f}}(k-1), \quad 0 < \alpha < 1 \tag{2}$$

In the experiments, the filter coefficient was set to $\alpha \approx 0.3$. The control structure employs a "feedforward + dual PID" strategy. The linear velocity command is given by:

$$v_{\mathrm{cmd}} = v_{\mathrm{ff}} + \Delta v \tag{3}$$

To prevent reverse movement, saturation limits were applied to both Δv and v_{cmd}.

The Steering PID takes the direction deviation D as input and outputs the steering velocity adjustment v_{turn}. To mitigate jitter, a deadband is introduced (setting $v_{\mathrm{turn}} = 0$ when $|D| < 0.03$). The final left and right wheel velocities are:

$$v_{\mathrm{L}} = v_{\mathrm{cmd}} - v_{\mathrm{turn}}, \quad v_{\mathrm{R}} = v_{\mathrm{cmd}} + v_{\mathrm{turn}} \tag{4}$$

Experiment 4 focuses on the "anti-interference hypothesis". A contrast experiment was designed where a candle interference was applied and compared with different modulation frequencies for anti-interference. The flame of the candle has a distinct radiation in the near-infrared band, which is a typical strong background IR interference source [7]. At the Leader end, the original emission structure is maintained, and three emission modes are generated by modifying the timer configuration:

- **DC Mode (0 Hz):** The emitter pin (`EMIT_PIN`) is set to `HIGH`, resulting in continuous conduction.
- **Standard PWM (approx. 490 Hz):** The default `Timer0` prescaler (64) is used with a 50% duty cycle (via `analogWrite(128)`).
- **High-Frequency PWM (approx. 3.9 kHz):** The `Timer0` prescaler is reduced to 8, maintaining the same duty cycle.

On the Follower side, active IR emissions are disabled to prevent interference, and signal reception relies exclusively on the left and right bump sensors (IR phototransistors). Wheel encoders are utilized for odometry, converting raw counts into linear displacement with a resolution of approximately 1 mm.

In each emission mode, a baseline experiment without the candle is conducted first: the Follower starts from a position almost close to the Leader, moves away from the Leader along a straight line, and calls the measurement function every time the cumulative displacement increases by approximately 1 mm. For each channel, multiple RC reads are performed, averaged, and a line of CSV is printed. Then, while keeping the route and step length as similar as possible, a candle is fixedly ignited on the side closer to the Follower between Leader and Follower, and the entire process is repeated. The curve under "interference" conditions is obtained.

Experiment 5 examines the distance hypothesis from the perspective of reading mode. It compares the distance response characteristics of the same line sensor in ADC and RC reading modes and checks for any interference when both are working simultaneously. According to the QTR sensor application note, the RC mode obtains the reflected light intensity by measuring the capacitor discharge time, while the simulation mode outputs a voltage approximately monotonically related to the light intensity [6]. In the experiment,

Leader continuously emits at a 3.9 kHz modulation. Follower is stationary and facing Leader. In the ADC mode of the online sensor, the relevant channels are configured as analog inputs. ADC values of DN2-DN5 are collected at several distance points (with a large distance step for long distances and a dense step for short distances) and averaged. Normalization is performed using the minimum and maximum ADC values in "no signal" and "close" conditions. Then, in the RC mode, the RC discharge time is detected at the same distance points and normalized using the same approach. In the interference test, the line sensor remains in the ADC mode. Sampling is repeated under two conditions: "only line operation" and "line + bump periodic RC reading simultaneously operating". The mean and variance of the ADC output are compared to determine if there are significant changes.

B. Discussion of Variables

1) Controlled Variables: The following controlled variables were standardized throughout the experiments to guarantee a fair comparison.

- **Experiment 1:** Two identical 3Pi+ robots, with the same body posture and alignment method. The same indoor environment and floor material. The same RC timeout (6000 μs) and the same max/min calibration process.
- **Experiment 2:** The speed of the Leader vehicle is constant at (40, 40). The indoor environment and lighting conditions are the same. The control algorithm structure and PID parameters are exactly the same in both modes. The sensor reading method is the RC mode and the timeout is consistent.
- **Experiment 3:** The hardware and environmental conditions, the Leader's movement mode and path, the sensor layout and reading method are the same as in Experiment 2.
- **Experiment 4:** Two identical 3Pi+ robots. The same bump receiving hardware and reading method. The same encoder parameters. The laboratory environment (avoiding additional IR sources) and the type, position, and height of the candles were standardized.
- **Experiment 5:** The Leader's output power and modulation frequency (fixed at 3.9 kHz). The Follower's posture and position (stationary and facing directly). The environmental lighting and background arrangement.

2) Independent Variable: The specific independent variables manipulated in each experiment are defined as follows.

- **Experiment 1:** The planar distance d between the Leader and the Follower. The testing range was 1–5 cm for the line sensor and 0.5–12.5 cm for the bump sensor.
- **Experiment 2:** The type of receiving sensor configuration: Bump-to-Bump (B→B) versus Bump-to-Line (B→L).
- **Experiment 3:** The controller structure and parameter settings. This includes the inclusion of feedforward velocity v_{ff}, the filter coefficient α, the gains for both Distance and Steering PIDs, and the deadband threshold.
- **Experiment 4:** The Leader's emission mode and modulation frequency, tested at three discrete levels: 0 Hz (DC), 490 Hz (Standard), and 3.9 kHz (High-Frequency).
- **Experiment 5:** The line sensor reading method (ADC vs. RC) and the multi-sensor configuration (Line-only vs. Line + Bump).

3) Dependent Variable(s): The key performance metrics and dependent variables measured in each experiment are listed below.

- **Experiment 1:** The raw RC discharge time T_{raw} and the normalized intensity S for both line and bump sensors. By analyzing the response curves across the distance domain and identifying the maximum effective range based on the "available signal threshold," the suitability of each sensor for ranging was evaluated.
- **Experiment 2:** Real-time normalized intensity $S(t)$ and the left-right differential $\Delta S(t)$. Key performance indicators included tracking continuity (target loss occurrence), effective signal range, and control stability (quantified by wheel speed jitter and the frequency of motor command reversals).
- **Experiment 3:** The steady-state relative distance between the Follower and Leader (indicated by filtered intensity S_{f}). The degree of fluctuation in linear velocity and left-right wheel velocities was recorded to detect significant oscillations or irrecoverable divergence. These metrics were used to identify parameter combinations that balance noise suppression with response speed.
- **Experiment 4:** The left and right normalized intensities $S_{\mathrm{L}}(d)$ and $S_{\mathrm{R}}(d)$, average intensity $S_{\mathrm{avg}}(d)$, and the curve deviation $\Delta S(d)$ under conditions with and without candle interference. These variables quantified the degradation in effective range and the increase in signal noise, thereby verifying the anti-interference hypothesis.
- **Experiment 5:** The normalized outputs $S_{\mathrm{ADC}}(d)$ and $S_{\mathrm{RC}}(d)$. Metrics included the maximum perceptible distance, output monotonicity, and noise levels (variance). Additionally, the offset and variance of the ADC output were analyzed to determine the optimal reading method for calibration and to assess cross-talk effects when multiple sensors operate simultaneously.

C. Discussion of Metrics

All experiments should adopt unified normalization and threshold definitions as much as possible. This facilitates horizontal comparisons.

Experiment 1: All RC readings are uniformly normalized using:

$$S = \frac{t_{\max} - t_{\mathrm{raw}}}{t_{\max} - t_{\min}}, S \in [0, 1] \tag{5}$$

The left and right channels of the bump are averaged to obtain the forward infrared intensity S_{bump}. By plotting the S–distance curve, we focus on observing whether there is a saturation zone at close range, whether it is approximately monotonic at medium range, and where it drops to the noise floor at long range. A threshold (e.g., $S \leq 0.2$) is defined, and the corresponding distance is defined as the maximum effective ranging distance. This is used for the parameter selection for subsequent following control.

Experiment 2: The control performance is mainly analyzed through four types of metrics:

- Signal effective range. The distance interval where $S(t) \geq 0.10$ during the following process.
- Stable distance determination ability. By observing the video of the relative position of the Follower and the Leader or the mileage record, as well as the fluctuation of $S(t)$.
- Speed smoothness. By calculating the standard deviation of the speeds of the left and right wheels and the number of times the PWM instruction symbol of the motor flips to determine whether there is snake-like jitter.
- Robustness. By counting the number of times "signal loss events" ($S < 0.10$ lasting for a certain period) occur in a single experiment.

These indicators are compared under the B→B and B→L modes. This can help determine which perception structure is more beneficial for the distance hypothesis and also provide a basis for subsequent turning experiments.

Experiment 3: The metrics used are divided into two parts: steady state and transient state.In the steady state aspect, after the Follower successfully locks behind the Leader and enters a relatively stable following mode, a time window is selected to calculate the mean and standard deviation of the filtered intensity S_f.This is used to estimate the relative distance and its fluctuations. At the same time, the mean and standard deviation of the speeds of the left and right wheels are calculated. The smoothness when walking in a straight line and the speed coordination during turning are evaluated. In the transient state aspect, attention is paid to the time from startup to entering the steady state. When the speed or trajectory of the Leader suddenly changes (for example, from a straight line to a gentle curve), whether there is a large overshoot in S_f and wheel speed, and the duration of the adjustment. The frequency of symbol reversal of the motor output under different parameter combinations and whether there is a "madness" behavior that requires manual intervention to recover are counted. Thus, the practicality of the controller is qualitatively evaluated.

Experiment 4: Quantitative comparison of anti-interference capabilities at different modulation frequencies. First, obtain the $S_{\mathrm{avg}}(d)$ curves under both candle-free and candle-present conditions for each mode. Define three indicators:

- Set the detection threshold T_{detect} (e.g., $T_{\mathrm{detect}} = 0.2$). Calculate the distance at which fist $S_{\mathrm{avg}}(d) < T$ in the presence of

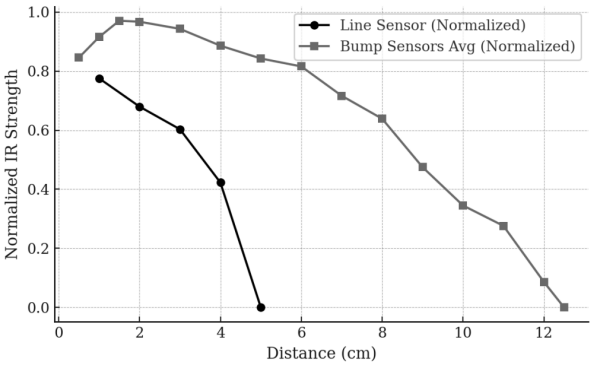

(a) Normalized IR Response vs. Distance

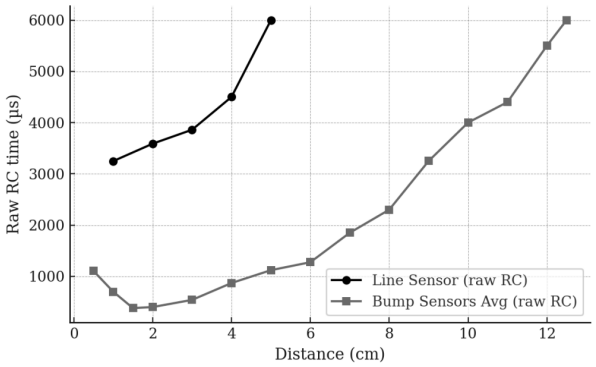

(b) Raw RC Readings vs. Distance

Fig. 1: Experimental results of IR ranging performance comparing Line and Bump sensors.

a candle as the maximum reliable detection distance for this mode under candle interference.

- Error area indicator. Numerically integrate $|S_{\text{avg,candle}}(d) - S_{\text{avg,baseline}}(d)|$ in the distance dimension to depict the cumulative interference degree.
- Noise indicator. Calculate the mean and standard deviation of the error within each distance or the entire distance segment to analyze the fluctuation size.

By comparing these indicators under the 0 Hz, 490 Hz, and 3.9 kHz modes, it can be seen whether high-frequency modulation is significantly superior to low-frequency or DC mode under strong IR interference, which is consistent with the conclusion in infrared positioning systems that modulation is used to improve the signal-to-noise ratio [3], [7].

Experiment 5: The core metrics are the distance response and noise characteristics of the two reading modes. The $S_{\text{ADC}}(d)$ and $S_{\text{RC}}(d)$ curves are plotted separately for ADC and RC modes. The monotonicity, the presence of long "quasi-linear segments", and the noise floor at long distances are examined. The maximum usable distance for each mode is given based on the farthest distance where $S \geq 0.10$ on the curves. In the linear degree analysis, simple functions can be fitted for the middle distance to evaluate the error. In the mutual interference test, the mean and variance changes of ADC output are compared when "only line operation" and "line + bump simultaneous operation" are used. If there is a significant deviation in the ADC output or a significant increase in noise when both operations are used, it indicates that the RC reading process affects the analog voltage reading, which is not conducive to using both types of readings simultaneously in practical following tasks. Through these indicators, it can be determined which mode is more suitable for distance calibration in this experiment, and also provides a basis for further expansion to multi-sensor fusion [6], [8].

IV. RESULTS

A. Experiment 1 & Experiment 5 (Based on $\mathcal{H}_1$)

1) Ranging Performance Comparison (Line vs. Bump): Data collected from Experiments 1 and 5 are presented in Fig. 1 below. These plots compare the raw and normalized responses of the bump and line sensors (y-axis) against the distance measured by the encoders (x-axis).

Line Sensor (Black Curve): The line sensor is very sensitive at short distance but the raw RC saturates at 5 cm (raw RC = 6000 μs). As a result, the normalized signal strength decreases rapidly to 0 beyond 4 cm. This effective range (< 5 cm) is too small to ensure reliable tracking.

Bump Sensor (Grey Curve): The bump sensor exhibits a large linear operating range. Its raw readings increase continuously from 0.5 to 12.5 cm with no saturation at low distances. At 10 cm depth, the normalized strength is over 0.35 showing great signal-to-noise ratio.

2) Mode Selection (ADC vs. RC): Experiment 5 also examined how signals should be read. The ADC mode showed a wide detection range (up to 55 cm) (as Table I shows), but the results showed that it was highly sensitive to angular offset (a 3° offset caused significant distance errors) and experienced hardware conflicts when running concurrently with bump sensors. On the other hand, although the RC mode is limited by physical reflection, it offers a steady and interference-free signal for control.

TABLE I: Normalized ADC Output vs. Distance (Line Sensor)

Distance (cm)	Normalized ADC (Arbitrary Units)	Distance (cm)	Normalized ADC (Arbitrary Units)
0	1.00	30	0.16
5	0.82	35	0.15
10	0.58	40	0.14
15	0.35	45	0.13
20	0.20	50	0.12
25	0.18	55	0.10

B. Experiment 2 (Based on $\mathcal{H}_3$)

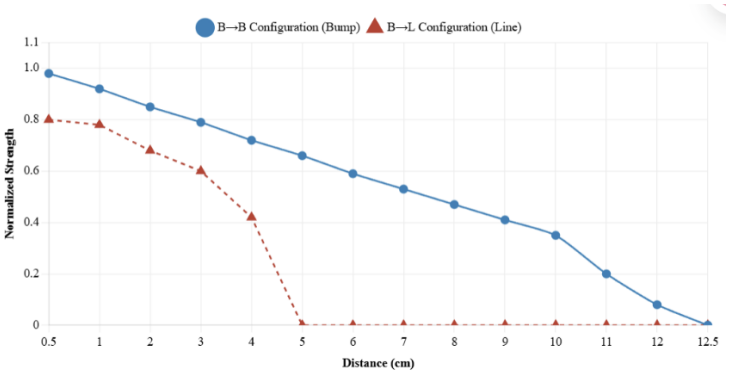

Fig. 2: Signal Strength vs. Distance (Configuration Comparison)

1) Steady-State Performance of the (B→B) model: Experimental results demonstrate exceptional robustness with the B→B configuration.

- **Signal Characteristics:** The normalized signal strength is depicted in Fig.2. It smoothly decays in a monotonic manner as the distance increases. The signal intensity is also higher than 0.30 for the range of distances between 0.5 and 10 cm. The strength remains high (> 0.60) in the core interval 2–8 cm. This means that its SNR is very good.
- **Following Performance:** The Leader has constant speed (40, 40). The Follower is capable of relatively stable closed-loop control. The outputs of distance PID and turning PID are continuous and smooth. There is no obvious overshoot or oscillation (Fig.3). The offset between the left and right bump sensor readings stays close to zero when the robot is moving straight. The front-facing sensors capture the geometric center of the Leader.

2) Analysis of unstabled Performance of the (B→L) model:

- **Sharp Signal Fall-off:** The response of the Line Sensor is very non-linear, as shown in Fig.2. Although a distinct signal

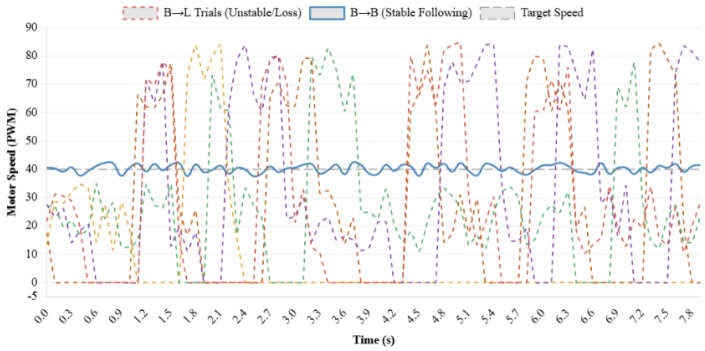

Fig. 3: Dynamic Motor Response (Stability Analysis)

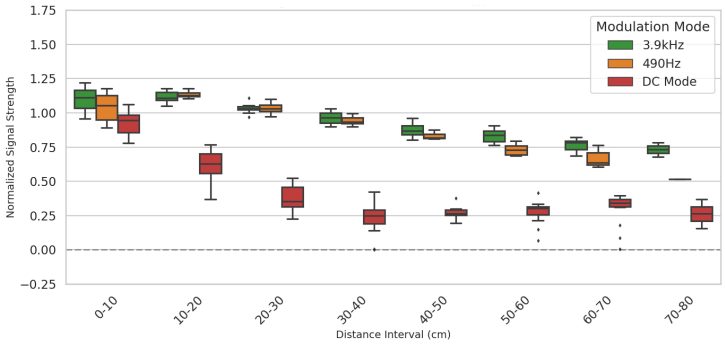

Fig. 4: Signal Variance by Distance

response between 1-3 cm can be easily observed, an abrupt decrease in signal intensity is observed between 4-5 cm (0.42 to 0). Consequently, the effective operating distance is limited to within 4.5 cm.

- **Control Instability:** Due to the downward-facing Field of View (FOV) of the Line Sensor, it does not look directly forward [1]. Therefore, if there is any increase in distance beyond 5 cm or slight heading errors, immediate signal loss occurs. This causes the PID control loop to enter a state of binary oscillation: motor commands fluctuate rapidly between "full-speed catch-up" and "signal-loss stop". As shown in Fig.3, the Follower exhibits erratic and violent motion, unable to follow smoothly the desired trajectory.

C. Experiment 3 (Based on $\mathcal{H}_1$ and $\mathcal{H}_3$)

1) Impact of Control Strategies on Stability: Results indicate that pure PID feedback is insufficient for smooth following.

- **Feedforward Control:** Without feedforward ($v_{\text{ff}} = 0$), the system relied entirely on error-driven commands, resulting in large fluctuations between zero and full speed and failing to establish a steady state. The introduction of feedforward ($v_{\text{ff}} = 35$) provided approximately 70% of the base power, allowing the PID controller to correct only minor deviations. This significantly improved response speed and suppressed overshoot.
- **Signal Processing & Deadband:** To address high-frequency noise in raw RC signals, a first-order low-pass filter ($\alpha = 0.3$) was applied to effectively smooth the input data. Additionally, a steering deadband ($|D| < 0.03$) was introduced to eliminate zigzag motion caused by minor sensor asymmetries, ensuring a stable straight trajectory.

2) Steady-State Performance Analysis: Under constant leader velocity (PWM -50), the optimized system demonstrated robust steady-state characteristics (see Table. II).

- **Distance Maintenance:** The normalized signal strength was maintained within the 0.52–0.53 range (approx. 6–7 cm physical distance) with no significant fluctuation.
- **Speed Synchronization:** The follower's motor PWM stabilized at 50 ± 2. This confirms that the closed-loop controller successfully compensated for hardware discrepancies, achieving precise velocity synchronization with the leader.
- **The results validate the Distance Hypothesis ($\mathcal{H}_1$):** Calibrated bump sensors possess sufficient linearity to support stable proportional control and turning Sensitivity Hypothesis ($\mathcal{H}_3$): By implementing a deadband to manage noise, the system can effectively use differential readings to correct heading errors and maintain formation stability.

D. Experiment 4 (Based on $\mathcal{H}_2$)

1) Signal Variance Analysis: Fig. 4 illustrates the distribution of normalized signal strength across distance intervals from 0 to 80 cm.

- **3.9 kHz (Green):** It shows the best stability. For all distance ranges, notably in the 0–40 cm range, the Interquartile Range (IQR) of the green boxes is very compressed. This shows that the high-frequency modulated signal remains tightly clustered with little measurement jitter despite flame interference.
- **DC Mode (Red):** Exhibits strong fluctuation. Notably in the 10–30 cm mid-range, the red boxes are elongated with a large spread between quartiles. This implies that the sensor readings randomly oscillate between signal and noise.
- **490 Hz (Orange)**: Performance falls somewhere in the middle. At close range it is acceptable, but at longer distances (60–70 cm) its box position is significantly lower than 3.9 kHz and has more dispersion.

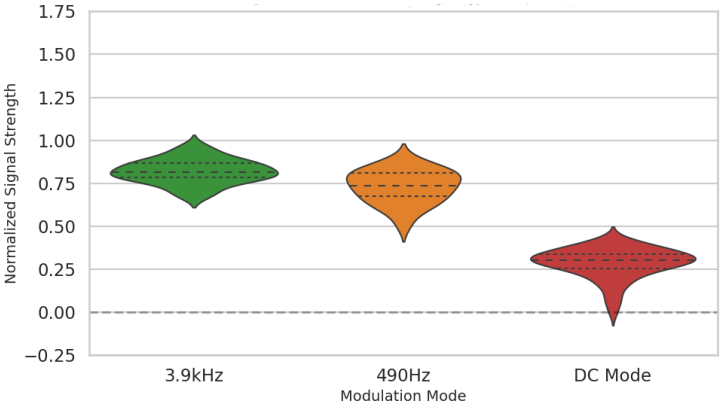

Fig. 5: Noise Distribution (Distance $>$ 40 cm)

2) Far-Field Noise Distribution: To investigate interference rejection in weak-signal regions, Fig. 5 analyzes the probability density of data collected at distances $>$ 40 cm.

- **3.9 kHz:** It shows a "flat and wide" distribution with a thick central peak located at a high level around 0.8. This morphology suggests that the data is tightly clustered, with little chance for data points to be distorted due to noise in the environment.
- **DC Mode:** In the plot, one finds a "slender and low-positioned" form with a center of mass which falls around 0.3, spreading across a wide range of 0.0–0.5. As such, we verify that in the far-field weak-signal area, the DC signal is practically dominated by the IR (noise) of flames so that the measured value has no physical meaning.

3) Hypothesis Verification: The experimental data confirms that the effectiveness of High-Frequency Filtering: 3.9 kHz modulation successfully isolates the signal from environmental thermal noise (typically DC or low-frequency) through spectral separation.

Conclusion: The Anti-Interference Hypothesis ($\mathcal{H}_2$) is validated. Compared to DC or 490 Hz, 3.9 kHz modulation significantly reduces signal variance, ensuring the credibility of ranging data in interference-prone environments.

V. DISCUSSION & CONCLUSION

This project focused on the Pololu 3Pi+ 32U4 robot. Under the Leader-Follower task, a systematic experiment was conducted on the infrared perception and control strategies.

$\mathcal{H}_1$: Experiment 1 first demonstrated that at the RC Timeout reading, the normalized intensity of the bump sensor decreased smoothly and monotonically with distance within the range of

TABLE II: Steady-State Following Log (Leader Speed: -50)

Time (ms)	Avg Strength	Filtered	Base Speed	Turn Adj	Motor L	Motor R
0	0.18	0.18	68	$+4$	64	72
200	0.30	0.25	62	$+2$	60	64
400	0.38	0.32	58	$+1$	57	59
600	0.45	0.39	54	0	54	54
800	0.50	0.45	52	-2	54	50
1000	0.52	0.49	51	-1	52	50
1200	0.53	0.51	50	0	50	50
1400	0.53	0.52	49	$+1$	48	50
1600	0.53	0.52	50	-1	51	49

0.5–10 cm. The intensity in the 2–8 cm range was greater than 0.60. This indicates a strong signal with low noise. When the distance exceeded approximately 11.5 cm, the intensity dropped below 0.10 and completely decayed at around 12–12.5 cm. The bottom line sensor responded effectively only within approximately 1–4.5 cm at the same RC reading mode. Between 4–5 cm, it almost "suddenly" dropped to 0. The fact that it is not suitable as a forward ranging sensor was verified in Experiment 5 [2].

In Experiment 5, the system was changed to read the forward infrared signal in ADC mode. And the Leader was driven by a PWM mode at 3.9 kHz (the effective frequency obtained after timer frequency division) by the PWM. The measurement showed that the ADC curve could still provide distinguishable signals varying with distance within the range of 10–55 cm under fixed posture and controllable background conditions. Although the nonlinearity was stronger in the medium and long distance sections and was sensitive to angle and reflection environment. However, in terms of "whether it can sense the presence of Leader and generate a meaningful intensity gradient", the ADC mode was significantly superior to the RC Timeout scheme in the long distance where it was almost completely "invisible". This is consistent with the common engineering experience of infrared proximity/reflective sensors that can achieve a ranging range of several tens of centimeters when using analog readings [9].

$\mathcal{H}_1$ was verified: Using ADC to read the forward infrared signal at a modulation of approximately 3.9 kHz. The usable ranging range can be expanded from approximately 0.5–12 cm under the bump sensor's RC mode to several tens of centimeters (about 55 cm in the experiment). However, it is necessary to note that the signals in the long distance section are significantly noisier and more dependent on posture and environment. Therefore, if it is to be directly used for closed-loop control, additional filtering and state estimation are required. Instead of simple thresholding or linear mapping.

$\mathcal{H}_2$: In Experiment 4 of the anti-interference capability test, three transmission modes were compared under the condition of infrared interference from a candle.

Before each experiment began, a manual calibration process was adopted. This ensured that the "Strength" was always scaled based on the "current environment". The 3.9 kHz modulation itself could already significantly suppress DC and low-frequency interference. The manual calibration further incorporated the remaining slow drift (such as changes in sunlight intensity and variations in the experiment table reflection) into the normalization process. This made the readings at the same distance more comparable over different time periods. In the fields of infrared communication and visible light communication, modulation + average voltage tracking and other methods are commonly used to suppress ambient light.

$\mathcal{H}_2$ was verified: Using 3.9 kHz modulation is the main factor for anti-interference. And "manual calibration before each start" played the role of "fine-tuning the zero point and amplitude" on this asis. In weak to moderate interference scenarios, it can reduce steady-state errors and threshold misjudgments caused by environmental changes. Pulse modulation is the source of the "qualitative change" in anti-interference capability. While manual calibration brings about "quantitative improvement". The combination of the two compared to "no calibration + direct current transmission" indeed achieved an observable improvement in robustness.

$\mathcal{H}_3$: Firstly, the replacement at the sensor level from "line" to "bump". The bump sensor is specifically designed for forward collision detection and left-right distinction. Its two independent receiving channels can provide a more natural "left/right intensity difference direction quantity". Meanwhile, it maintains a high signal-to-noise ratio within the range of 0.5–10 cm [2]. Experiment 2 indicates that in the B-emit B-receive configuration, even with the initial version of PID, the Follower can maintain basic distance and steering capabilities within a range of 2–8 cm. While the B-emit L-receive configuration is almost completely ineffective. Therefore, switching from the "line" sensor to the "bump" sensor at the control level itself significantly improves the continuity and usability of direction measurement. Secondly, at the control level: the introduction of feedforward, first-order low-pass, and dead zone PID improvements [10].

Experiment 3 quantitatively shows that under the improved control structure, the Follower can maintain a smaller distance error and smoother speed changes in both straight-line following and turning tracking.

$\mathcal{H}_3$ has been verified: the improvement in turning stability not only comes from using a more suitable direction sensor. It also clearly demonstrates the positive effects brought about by the PID algorithm structure and parameter optimization.

REFERENCES

[1] J. Hirata-Acosta, J. Pliego-Jiménez, C. Cruz-Hernández, and R. Martínez-Clark, "Leader-follower formation control of wheeled mobile robots without attitude measurements," *Applied Sciences*, vol. 11, no. 12, p. 5639, Jun 2021, doi: 10.3390/app11125639.

[2] Pololu Corporation, *Pololu 3pi+ 32U4 User's Guide*, Pololu Corporation, 2022, accessed: Dec. 02, 2025. [Online]. Available: https://www.pololu.com/docs/0J83

[3] E. M. Gorostiza, J. L. Lázaro Galilea, F. J. Meca Meca, D. Salido Monzú, F. Espinosa Zapata, and L. Pallarés Puerto, "Infrared sensor system for mobile-robot positioning in intelligent spaces," *Sensors*, vol. 11, no. 5, pp. 5416–5438, May 2011, doi: 10.3390/s110505416.

[4] R. A. Khan, M. A. Qureshi, and S. Saeed, "Vision based navigation for a mobile robot with different field of views," *arXiv preprint arXiv:0906.4973*, Jun 2009, doi: 10.48550/arXiv.0906.4973.

[5] A. Latif, A. Z. Arfianto, H. A. Widodo, R. Rahim, and E. T. Helmy, "Leader-follower formation tracking of multiple mobile robots with constant leader velocity," *Journal of Physics: Conference Series*, vol. 1569, no. 3, p. 032084, jul 2020, doi: 10.1088/1742-6596/1569/3/032084.

[6] Pololu Corporation, *Pololu QTR Reflectance Sensor Application Note*, Pololu Corporation, accessed: Dec. 02, 2025. [Online]. Available: https://www.pololu.com/docs/0j13/all

[7] R. Elagib, F. Mitri, A. De Iacovo, A. Ballabio, J. Frigerio, G. Isella, and L. Colace, "Flame detector based on a ge-on-si photodetector with a voltage tunable spectral response," *IEEE Access*, vol. 13, pp. 174 071–174 077, 2025, doi: 10.1109/ACCESS.2025.3618306.

[8] Pololu Corporation, *Arduino Library for the Pololu QTR Reflectance Sensors*, Pololu Corporation, accessed: Dec. 02, 2025. [Online]. Available: https://www.pololu.com/docs/0j19/all

[9] Sharp Corporation, *Distance Measuring Sensor GP2Y0A21YK0F Datasheet*, Sharp Corporation, Dec 2006, sheet No.: E4-A00201EN. Accessed: Dec. 02, 2025. [Online]. Available: https://global.sharp/products/device/lineup/data/pdf/datasheet/gp2y0a21yk_e.pdf

[10] I.-S. Choi and J.-S. Choi, "Leader-follower formation control using PID controller," in *Intelligent Robotics and Applications*, C.-Y. Su, S. Rakheja, and H. Liu, Eds. Berlin, Heidelberg: Springer, 2012, pp. 625–634, doi: 10.1007/978-3-642-33515-0$_6$1.